OPEN

Correspondence and
requests for materials
should be addressed to
U.S. (udo.
schwingenschlogl@
kaust.edu.sa)

Superior thermoelectric response in the 3R phases of hydrated Na$_x$RhO$_2$

Y. Saeed, N. Singh & U. Schwingenschlögl

Physical Science & Engineering division, KAUST, Thuwal 23955-6900, Kingdom of Saudi Arabia.

Density functional theory is used to investigate the thermoelectric properties of the 3R phases of Na$_x$RhO$_2$ for different Na vacancy configurations and concentrations. As compared to the analogous 2H phases, the modified stacking of the atomic layers in the 3R phases reduces the interlayer coupling. As a consequence, the 3R phases are found to be superior in the technologically relevant temperature range. The Rh $d_{3z^2-r^2}$ orbitals still govern the valence band maxima and therefore determine the transport properties. A high figure of merit of 0.35 is achieved in hydrated Na$_{0.83}$RhO$_2$ at 580 K by water intercalation, which is 34% higher than in the non-hydrated phase.

Thermoelectric materials are required for power generation from waste heat as well as for refrigeration. However, the practical application is limited by the low efficiency of thermoelectric devices as compared to traditional fuel power generators and compressor-based refrigerators[1]. A high performance thermoelectric material has to be a good electrical and poor thermal conductor and, at the same time, has to possess a high Seebeck coefficient[2]. The efficiency is determined by the dimensionless figure of merit $zT = \sigma S^2 T/\kappa$, where σ is the electrical conductivity, S is the Seebeck coefficient, T is the temperature, and κ is the thermal conductivity. According to the classical semiconductor theory, heavily doped semiconductors with carrier concentrations of 10^{19} to 10^{21} cm^{-3} in general are promising candidates for high zT materials[3].

The discovery of a high Seebeck coefficient ($S \sim 100$ μV/K at 300 K) in Na$_x$CoO$_2$ has attracted considerable attention about a decade ago[4,5]. It has been predicted that the two-dimensional structure with alternatively stacked Na and CoO$_2$ layers plays an important role for the high zT of Na$_{0.5}$CoO$_2$[6]. Later, Kuroki et al.[7] have argued that the peculiar pudding mold shape of the valence band of Na$_x$CoO$_2$ is responsible for the high zT (with high σ), see also[8]. Interestingly, Takada et al.[9] have demonstrated that the compounds can be readily hydrated to form Na$_x$CoO$_2 \cdot y$H$_2$O, maintaining the CoO$_2$ layers, but with a considerably expanded crystal c-axis to accomodate the intercalated water. The electronic structures of hydrated and non-hydrated Na$_x$CoO$_2$ have been studied by first principles calculations in Ref. 10.

Analogous compounds with Rh in place of Co are also good thermoelectric materials, since the octahedrally coordinated ions Rh^{3+} (4d^6) and Rh^{4+} (4d^5) show similar electronic structures as Co^{3+} (3d^6) and Co^{4+} (3d^5), but exhibit reduced correlation effects[11–14]. Experiments could not verify any magnetic ordering in Na$_x$RhO$_2$[15]. In general, the Rh 4d orbitals are spatially more dispersed than the Co 3d orbitals, which may result in an increased mobility of the charge carriers. Varela et al.[16] have synthesized Na$_x$RhO$_2$ as solid solutions composed of nanometric particles of the α-NaFeO$_2$ structure type (space group $R\bar{3}m$, no. 166) for $x = 0.70$ and 0.85. The 3R structure of Na$_x$RhO$_2$ contains three layers of RhO$_6$ octahedra per unit cell. Using the hexagonal setting of the $R\bar{3}m$ space group, the c-axis of the unit cell has a length of typically 18 Å, while the length of the a-axis strongly depends on the specific transition metal cation.

It is important to notice that the layered oxides LiRhO$_2$, NaRhO$_2$, and KRhO$_2$ can form hydrated, i.e., water intercalated, phases[17] with an elongated c-axis. For Na$_x$RhO$_2$ it has been shown that the water intercalation and the elongated unit cell result in a decrease of the resistivity[18]. Accordingly, in Ref. 19 a colossal thermoelectric powerfactor has been demonstrated theoretically for K$_{7/8}$RhO$_2$ in the case of hydration, which is nowadays triggering various experimental efforts[20,21]. From a practical point of view the results reported on K$_{7/8}$RhO$_2$ are limited by the fact that the optimal thermoelectric performance is achieved below usual operation temperatures[19]. In this context we propose to switch from the 2H phase (two RhO$_6$ layers per unit cell with a hexagonal structure of space group $P6_3/mmc$, no. 194, and $c \sim 12$ Å) to the 3R phase, as one may speculate that the thermoelectric properties are modified by the different stacking (larger band gap in the 3R phases[22]). Accordingly, we study in the following the thermoelectric properties of both non-hydrated ($c = 15.54$ Å) and hydrated ($c = 20.85$ Å) 3R-Na$_x$RhO$_2$, for which we first determine the lowest energy structures for $x = 0.75$ and 0.83. Afterwards we analyze

the effects of hydration on the transport properties in the temperature range from 300 K to 800 K and demonstrate the great potential of the 3R-Na_xRhO_2 class of materials as thermoelectrics. The 3R phase turns out to be clearly superior to the 2H phase in the technologically relevant temperature range.

Results

We start from the experimental lattice parameters $a = 3.09$ Å and $c = 15.54$ Å of $NaRhO_2$[16] and construct a $2 \times 2 \times 1$ supercell. Afterwards we remove two Na atoms from different sites to obtain $Na_{0.83}RhO_2$. These configurations are named A1, A2, and A3. Similarly, we remove three Na atoms to obtain $Na_{0.75}RhO_2$ and name these configurations B1, B2, and B3. All the structures under investigation are shown in Fig. 1. The formation energy is calculated for each configuration by the relation

$$E_{Formation} = E_{Defect} - E_{Pristine} + 12(1-x)E_{Na}.$$

Here $E_{Pristine}$ is the total energy of a supercell of pristine $NaRhO_2$. In addition, E_{Defect} and E_{Na} are the total energies of the defective supercell and of the isolated Na atom, respectively. The energy of an isolated atom is calculated by placing the atom in a cubic cell of 20 Å side length.

The formation energies of configurations A1, A2, and A3 amount to 7.83 eV, 6.73 eV, and 6.65 eV, respectively, and those of configurations B1, B2, and B3 to 11.54 eV, 10.34, and 9.90 eV. These results show that for $Na_{0.75}RhO_2$ and $Na_{0.83}RhO_2$, respectively, the A3 and B3 configuration has the lowest energy. The latter structures are characterized by maximal distances between the defects, which indicates that Na vacancies do not cluster in Na_xRhO_2, at least not in the two systems under investigation. Moreover, a minimum energy of 6.65 eV is required for creating two Na vacancies in $NaRhO_2$ and an energy of 9.90 eV for creating three vacancies. In the following, we will discuss only the lowest energy structures A3 and B3 unless otherwise mentioned. In pristine $NaRhO_2$ the Rh–O bond length amounts to 2.07 Å and the thickness of the RhO_6 layer is 2.11 Å,

which is larger than the thickness of the CoO_6 layer (1.82 Å) in $NaCoO_2$. Moreover, the bond angle $\angle Rh-O-Rh = 96.5°$ is smaller than the bond angle $\angle Co-O-Co = 98.35°$. Next to vacancies the RhO_6 octahedra shrink slightly (the Rh–O bond lengths decrease by 0.02–0.05 Å), because the interlayer coupling through the Na atoms is reduced and the RhO_6 octahedra thus become a bit more compact, which also influences the electronic and thermoelectric properties of the material.

We determine the effects on the electronic band structure and corresponding density of states (DOS), for $NaRhO_2$, $Na_{0.83}RhO_2$, and $Na_{0.75}RhO_2$ in Fig. 2. $NaRhO_2$ has a indirect band gap of 1.33 eV along the Γ–M high symmetry direction. The valence band mainly is formed by the Rh $4d$ t_{2g} states and shows a total width of a bit less than 2 eV. This value is comparable to the bandwidth of $NaCoO_2$, even though $4d$ orbitals are more extended than $3d$ orbitals and thus usually exhibit higher bandwidths. The conduction band minimum belongs almost purely to the e_g states. On the other hand, the valence band maximum, which is particularly important as it determines the consequences of hole doping, is due to the $d_{3z^2-r^2}$ orbital. The electronic band structures obtained for configurations A3 and B3 are similar to the pristine case, except for the introduction of holes with densities of $8.8 \cdot 10^{20}$ cm^{-3} (A3) and $8.7 \cdot 10^{20}$ cm^{-3} (B3). Besides the characteristic peak approximately 0.2 eV below the Fermi energy, the DOS of prsitine $NaRhO_2$ shows $d_{3z^2-r^2}$ states down to -0.75 eV and between -1 eV and -1.75 eV, which is similar for $Na_{0.83}RhO_2$ and $Na_{0.75}RhO_2$ except for the states at the Fermi level, which have different effective masses and consequently result in different Seebeck coefficients.

The transport properties of hydrated and non-hydrated $Na_{0.83}RhO_2$ and $Na_{0.75}RhO_2$ are addressed in Fig. 3. We show the Seebeck coefficient and figure of merit for the temperature range from 300 K to 800 K. The Seebeck coefficient is positive in the whole range, indicating that the carriers are holes. We obtain room temperature values of $S = 63$ μVK^{-1} and $S = 37$ μVK^{-1} for non-hydrated $Na_{0.83}RhO_2$ and $Na_{0.75}RhO_2$, respectively. For hydrated
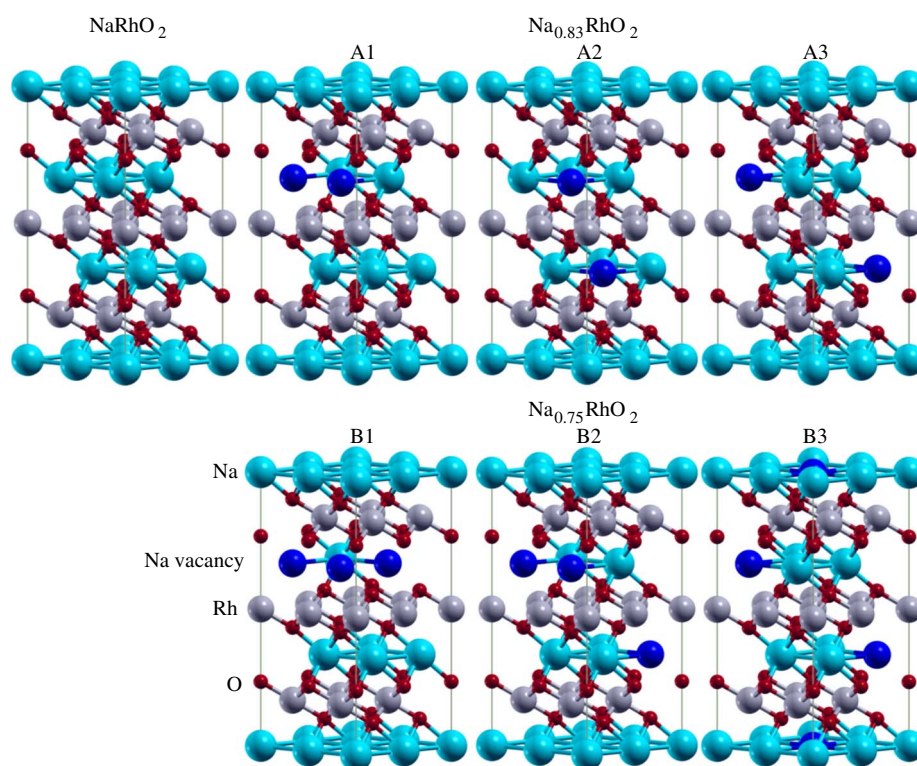

Figure 1 | Atomic structures of $NaRhO_2$, $Na_{0.83}RhO_2$, and $Na_{0.75}RhO_2$ for different vacancy configurations.

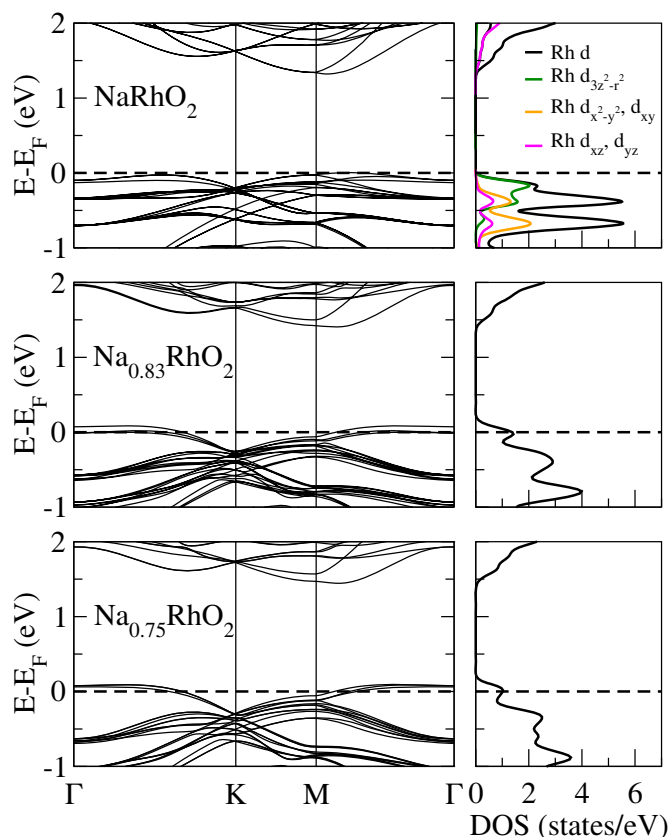**Figure 2 | Band structures and Rh 4d DOSs of NaRhO$_2$, Na$_{0.83}$RhO$_2$ (non-hydrated), and Na$_{0.75}$RhO$_2$ (non-hydrated).**

and non-hydrated Na$_{0.83}$RhO$_2$ the Seebeck coefficient behaves rather similarly as a function of the temperature, except for the high temperature range where hydration reduces S. Moreover, according to Figs. 3(c) and 3(d), zT at 300 K (room temperature) amounts to 0.16 and 0.06 in the two systems. The former value is twice that found for Na$_{0.85}$CoO$_2$ and Na$_{0.88}$CoO$_2$ in Ref. 5. Starting from almost the same value at 300 K, hydration enhances zT over the whole temperature range, such that at 800 K a value of about 0.4 is reached. At 580 K a maximal increment of 34% due to hydration is achieved. For Na$_{0.75}$RhO$_2$ the Seebeck coefficient increases at 300 K from

37 μVK^{-1} to 51 μVK^{-1} under hydration, where this increment of about 30% remains essentially constant over the whole temperature range. A similar effect is also found for zT. At 800 K again a value of about 0.4 is reached.

The enhancement of S under hydration results in higher zT values. While the gross shape of the band structure changes little under hydration, see Fig. 4, the Rh 4d bands become flatter in a narrow region around the Fermi level. This fact causes the effective masses and therefore the resistivity to increase and results in a higher Seebeck coefficient. Moreover, the long c-axis of the hydrated phase
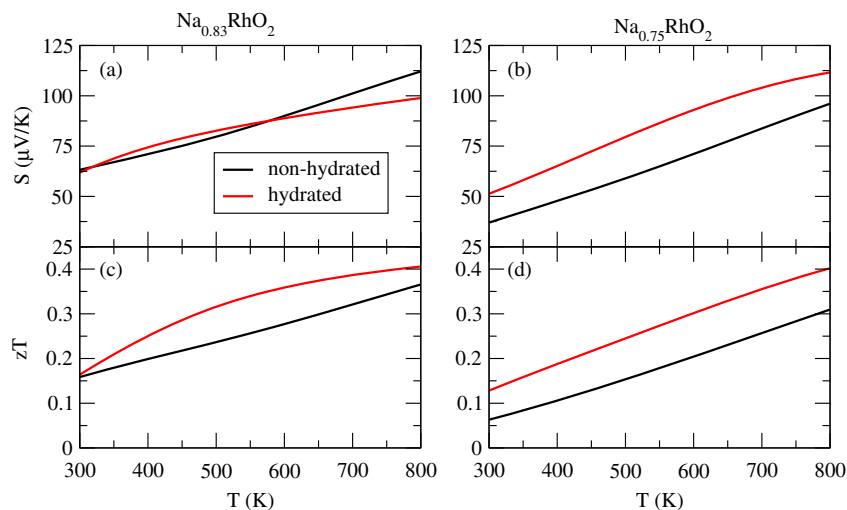

Figure 3 | Transport properties of non-hydrated and hydrated Na$_{0.83}$RhO$_2$ and Na$_{0.75}$RhO$_2$ as functions of the temperature. (a), (b) Seebeck coefficient and (c), (d) figure of merit.

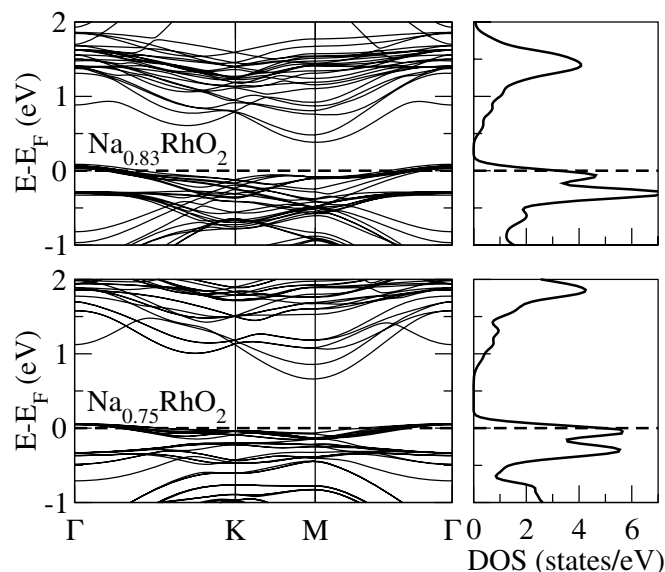**Figure 4 | Band structures and Rh 4*d* DOSs of hydrated Na$_{0.83}$RhO$_2$ and Na$_{0.75}$RhO$_2$.**

causes the Rh 4*d* states to shift down in energy towards the Fermi level, because the Rh–O overlap is reduced (increased bond length of 2.2 Å). In order to study possible disorder of the vacancies we have also calculated the Seebeck coefficient (not shown) of the higher energy configurations A1, A2, B1, and B2. For A2 and B2 the results are close to the values of the respective lowest energy configurations, because both have the vacancies in different RhO$_6$ layers. In contrast, concentration of vacancies in the same RhO$_6$ layer results in a significant reduction of S, which is, however, highly unlikely as certified by the previously listed formation energies.

Discussion

The Na$_x$RhO$_2$ oxides are found to form a new class of materials with exciting thermoelectric features, even outperforming the 2H phases of the K$_x$RhO$_2$ system. In the latter the optimal thermoelectric performance is achieved at low temperature, whereas the modified stacking of the atomic layers in the novel 3R phases of Na$_x$RhO$_2$ results in a reduced interlayer coupling and, in turn, in a dramatically enhanced thermoelectric response in the technologically relevant high temperature range. We have also demonstrated that Na vacancies in Na$_x$RhO$_2$ avoid clustering and that the RhO$_6$ octahedra are modified depending on the amount of Na deficiency. Analysis of the induced changes in the DOS close to the Fermi level indicates that mainly Rh$^{3+\delta}$ $d_{3z^2-r^2}$ states control the transport properties of the compounds. A high zT value of 0.35 at 580 K is achieved in hydrated Na$_{0.83}$RhO$_2$ due to the enhanced effective mass of the charge carriers. In general, zT can be further increased by reduction of the Na vacancy concentration to increase the resistivity.

Methods

We study the effects of Na deficiency and hydration on the band structure of NaRhO$_2$ using density function theory as implemented in the WIEN2k package[23]. The exchange-correlation potential is parametrized in the generalized gradient approximation[24]. We fully optimize the structure of Na$_x$RhO$_2$ for $x = 1$, 0.83, and 0.75, considering $2 \times 2 \times 1$ supercells, until the atomic forces reach values of less than 10 mRyd/a_B. For the wave function expansion inside the atomic spheres a maximal angular momentum of $\ell_{max} = 12$ is employed and a plane-wave cutoff of $R_{mt}K_{max} = 7$ with $G_{max} = 24$ is used. Self-consistency is assumed when the total energy variation is less than 10^{-4} Ry. The transport behavior is investigated using BoltzTraP[25], which employs a methodology that previously has demonstrated to yield quantitatively accurate values for the thermoelectric properties of metals and doped semiconductors[26–29]. It is based on semi-classical Boltzmann theory within the constant relaxation time approximation, i.e., the scattering rate is assumed to be independent of momentum and energy. This approximation allows the thermopower to be directly calculated from the band structure as a function of the carrier concentration and

temperature[30]. We note that it has been demonstrated for layered oxides isostructural to the present compound that at elevated temperatures the lattice part of the thermal conductivity can be neglected as compared to the electronic part[31]. We use a k-mesh of $7 \times 7 \times 2$ points for the band structure and density of states (DOS) and a dense k-mesh of $18 \times 18 \times 18$ points for the thermoelectric calculations.

1. DiSalvo, F. J. Thermoelectric cooling and power generation. *Science* **285**, 703–706 (1999).
2. Bell, L. E. Cooling, heating, generating power, and recovering waste heat with thermoelectric systems. *Science* **321**, 1457–1461 (2008).
3. Mahan, G., Sales, B. & Sharp, J. Thermoelectric materials: New approaches to an old problem. *Phys. Today* **50**, 42–47 (1997).
4. Terasaki, I., Sasago, Y. & Uchinokura, K. Large thermoelectric power in NaCo$_2$O$_4$ single crystals. *Phys. Rev. B* **56**, R12685–R12687 (1997).
5. Lee, M. *et al.* Large enhancement of the thermopower in Na$_x$CoO$_2$ at high Na doping. *Nat. Mater.* **5**, 537–540 (2006).
6. Koshibae, W., Tsutsui, K. & Maekawa, S. Thermopower in cobalt oxides. *Phys. Rev. B* **62**, 6869–6872 (2000).
7. Kuroki, K. & Arita, R. "Pudding mold" band drives large thermopower in Na$_x$CoO$_2$. *J. Phys. Soc. Jpn.* **76**, 083707 (2007).
8. Saeed, Y., Singh, N., Parker, D. & Schwingenschlögl, U. Thermoelectric performance of electron and hole doped PtSb$_2$. *J. Appl. Phys.* **113**, 163706 (2013).
9. Takada, K. *et al.* Superconductivity in two-dimensional CoO$_2$ layers. *Nature* **422**, 53–55 (2003).
10. Johannes, M. D. & Singh, D. J. Comparison of the electronic structures of hydrated and unhydrated Na$_x$CoO$_2$: The effect of H$_2$O. *Phys. Rev. B* **70**, 014507 (2004).
11. Klein, Y., Hébert, S., Pelloquin, D., Hardy, V. & Maignan, A. Magnetoresistance and magnetothermopower in the rhodium misfit oxide [Bi$_{1.95}$Ba$_{1.95}$Rh$_{0.1}$O$_4$][RhO$_2$]$_{1.8}$. *Phys. Rev. B* **73**, 165121 (2006).
12. Shibasaki, S., Kobayashi, W. & Terasaki, I. Transport properties of the delafossite Rh oxide Cu$_{1-x}$Ag$_x$Rh$_{1-y}$Mg$_y$O$_2$: Effect of Mg substitution on the resistivity and Hall coefficient. *Phys. Rev. B* **74**, 235110 (2006).
13. Lee, K. W. & Pickett, W. E. Chemical differences between K and Na in alkali cobaltates. *Phys. Rev. B* **76**, 134510 (2007).
14. Kobayashi, W., Hébert, S., Pelloquin, D., Pérez, O. & Maignan, A. Enhanced thermoelectric properties in a layered rhodium oxide with a trigonal symmetry. *Phys. Rev. B* **76**, 245102 (2007).
15. Krockenberger, Y. *et al.* Neutron scattering and magnetic behavior of Na$_x$RhO$_2$. *Physica C* **460–462**, 468–470 (2007).
16. Varela, A., Parras, M. & González-Calbet, J. M. Influence of Na Content on the Chemical Stability of Nanometric Layered Na$_x$RhO$_2$ ($0.7 \le x \le 1.0$). *Eur. J. Inorg. Chem.* **2005**, 4410–4416 (2005).
17. Mendiboure, A., Eickenbusch, H. & Schollhorn, R. Layered alkali rhodium oxides A$_x$RhO$_2$: Topotactic solvation, exchange, and redox reactions. *J. Solid State Chem.* **71**, 19–28 (1987).
18. Park, S. *et al.* Synthesis and characterization of Na$_{0.3}$RhO$_2$ · 0.6H$_2$O – a semiconductor with a weak ferromagnetic component. *Solid State Commun.* **135**, 51–56 (2005).
19. Saeed, Y., Singh, N. & Schwingenschlögl, U. Colossal thermoelectric power factor in K$_{7/8}$RhO$_2$. *Adv. Funct. Mater.* **22**, 2792–2796 (2012).

20. Yao, S. H. *et al.* Structure and physical properties of $K_{0.63}RhO_2$ single crystals. *AIP Advances* **2**, 042140 (2012).

21. Zhang, B.-B. *et al.* High temperature solution growth, chemical depotassiation and growth mechanism of K_xRhO_2 crystals. *Cryst. Eng. Comm.* **15**, 5050–5056 (2013).

22. Okada, S., Terasaki, I., Okabe, H. & Matoba, M. Transport properties and electronic states in the layered thermoelectric rhodate $(Bi_{1-x}Pb_x)_{1.8}Ba_2Rh_{1.9}O_y$. *J. Phys. Soc. Jpn.* **74**, 1525–1528 (2005).

23. Blaha, P., Schwarz, K., Madsen, G., Kvasicka, D. & Luitz, J. WIEN2k, An augmented plane wave plus local orbitals program for calculating crystal properties (TU Vienna, Vienna, 2001).

24. Perdew, J. P., Burke, K. & Ernzerhof, M. Generalized gradient approximation made simple. *Phys. Rev. Lett.* **77**, 3865–3868 (1996).

25. Madsen, G. K. H. & Singh, D. J. BoltzTraP. A code for calculating band-structure dependent quantities. *Comput. Phys. Commun.* **175**, 67–71 (2006).

26. Scheidemantel, T. J., Ambrosch-Draxl, C., Thonhauser, T., Badding, J. V. & Sofo, J. O. Transport coefficients from first-principles calculations. *Phys. Rev. B* **68**, 125210 (2003).

27. Madsen, G. K. H., Schwarz, K., Blaha, P. & Singh, D. J. Electronic structure and transport in type-I and type-VIII clathrates containing strontium, barium, and europium. *Phys. Rev. B* **68**, 125212 (2003).

28. Singh, D. J. Electronic and thermoelectric properties of $CuCoO_2$: Density functional calculations. *Phys. Rev. B* **76**, 085110 (2007).

29. Zhang, L., Du, M.-H. & Singh, D. J. Zintl-phase compounds with $SnSb_4$ tetrahedral anions: Electronic structure and thermoelectric properties. *Phys. Rev. B* **81**, 075117 (2010).

30. Singh, D. J. & Mazin, I. I. Calculated thermoelectric properties of La-filled skutterudites. *Phys. Rev. B* **56**, R1650–R1653 (1997).

31. Satake, A., Tanaka, H., Ohkawa, T., Fujii, T. & Terasaki, I. Thermal conductivity of the thermoelectric layered cobalt oxides measured by the Harman method. *J. Appl. Phys.* **96**, 931–933 (2004).

Author contributions

Additional information